ELSEVIER

Journal of Photochemistry and Photobiology B: Biology 38 (1997) 234–240

Journal of PHOTOCHEMISTRY AND PHOTOBIOLOGY B:BIOLOGY

Reconstruction of in vivo skin autofluorescence spectrum from microscopic properties by Monte Carlo simulation

Haishan Zeng [a,*], Calum MacAulay [a], David I. McLean [b,c,d], Branko Palcic [a]

[a] *Cancer Imaging Department, British Columbia Cancer Research Centre, 601 West 10th Avenue, Vancouver, BC, Canada V5Z 1L3*

[b] *Division of Dermatologic Oncology, British Columbia Cancer Agency, Vancouver, BC, Canada V5Z 1L3*

[c] *Division of Dermatology, Faculty of Medicine, University of British Columbia, Vancouver, BC, Canada V5Z 1L3*

[d] *Skin Care Centre, Vancouver Hospital and Health Sciences Centre, Vancouver, BC, Canada V5Z 1L3*

Received 9 July 1996; accepted 4 November 1996

Abstract

The in vivo skin autofluorescence spectrum was reconstructed by Monte Carlo simulation using microscopic fluorophore distributions and intrinsic fluorescence spectra measured from excised skin tissue sections as well as employing published skin tissue optical parameters. The theoretical modeling took into account the light–tissue interactions of scattering, absorption, and regeneration of fluorescence photons. The modification of the intrinsic spectra by tissue optical properties to generate the in vivo spectrum observed at the tissue surface can be represented by a fluorescence detection efficiency function (η) which equals the integral of the product of the excitation light distribution inside the tissue and the fluorescence escape efficiency. Comparison of the reconstructed in vivo spectrum with the measured spectra showed good agreement, outside of the blood absorption bands, suggesting that (i) the theoretical modeling, (ii) the skin optical parameters used, and (iii) the measured microscopic morphology and spectral data are consistent. The divergence which exists over the strong blood absorption wavelength band (530–600 nm) suggests that the effect of blood contents on in vivo tissue optical properties deserves further investigations.

Keywords: Tissue autofluorescence; Microscopic spectral analysis; Fluorophore micro-distribution; Monte Carlo simulation; Human skin

1. Introduction

The in vivo spectra of tissue autofluorescence emissions are determined by the microscopic properties of the tissue. The excitation light distribution inside the tissue determines which fluorophores inside the tissue will be excited to fluoresce. According to radiative transfer theory [1,2], the microscopic properties of tissue governing the light propagation can be described by three transport parameters: the absorption coefficient μ_a, the scattering coefficient μ_s, and the scattering anisotropy, g. In addition, the microscopic fluorophore distribution inside the tissue determines the origin of the in vivo autofluorescence signals, while the intrinsic emission spectra of the fluorophores set the predominant profile of the observed in vivo spectra. Finally, the observed in vivo spectra are also affected by the reabsorption and scattering of the tissue on the fluorescence photons as they attempt to escape out of the tissue [3–7]. A complete understanding of the in vivo spectra must therefore take into account all the above factors.

The transport parameters of skin tissue have been studied for many years and were summarized in Refs. [8] and [9]. Recently, we have systematically characterized the autofluorescence emission properties of normal human skin [7,10,11] including in vivo spectra and in vitro fluorophore micro-distribution and intrinsic spectra. Our results demonstrated that the skin fluorophore distribution is not uniform, but has a layered structure, indicating that the uniform fluorophore distribution used in previous theoretical modeling of fluorescence measurements is not appropriate for skin tissue. All previous models [4,12–16] assumed uniform fluorophore distribution in a semi-infinite medium or used average fluorophore distributions derived from macroscopic measurements. To better understand the skin autofluorescence process, in this work, we reconstruct the in vivo autofluorescence spectrum of skin by Monte Carlo simulation using microscopic scale fluorophore distributions and measured local intrinsic spectra in combination with published skin optical parameters.

* Corresponding author. Tel.: +1 604 877 6010 ext. 3011; fax: +1 604 875-6857; e-mail: hzeng@physics.ubc.ca

PII S1011-1344(96)00008-5

2. Materials and methods

The setup used for in vivo spectral measurement has been described in detail in Refs. [6] and [10]. A 442 nm He–Cd laser (Ominichrome, Chino, CA, USA) output was coupled into a 400 μm fiber with microlens to illuminate the measurement skin site. The microlens attached to the fiber was used to achieve a 10 mm diameter uniform illumination spot. The excited autofluorescence light was collected by a large core (1000 μm) diameter fiber and transmitted to an Optical Multichannel Analyzer (OMA, EG and G Princeton Applied Research, Princeton, NJ, USA) for spectral analysis. The pick-up spot size was measured to be 3 mm in diameter by conducting light in the reverse direction into the collection fiber. The two fibers were held by a fiber holder which keeps the two fibers so-centred and allows the illumination and detection angles to be varied. In this study, the illumination fiber is positioned nearly perpendicular to the skin surface, while the collection fiber is positioned at an angle of 30° with respect to the illumination fiber. A 470 nm long pass filter was inserted into the light path on the OMA side to block the scattered excitation laser light while allowing the longer wavelength fluorescence light to pass through. All acquired spectra were both wavelength and intensity calibrated. In this study, we measured the autofluorescence spectra at multiple sites on the normal skin of eight healthy volunteers of Caucasian and Asian origin.

The MSP used for microscopic spectral analyses of in vitro skin tissue sections has been described in detail in Ref. [17]. Fresh skin tissue samples were frozen and cut into sections of about 10 μm thick (kept unstained and unfixed) and then placed on glass microscope slides for examination. Light from a 442 nm, 100 mW, He–Cd laser was conducted to a multi-port microscope (Nikon, Japan) to illuminate the skin tissue slide and to excite the emission of autofluorescence. The microscopic fluorescence image was recorded by a three-chip CCD (charge coupled device) color camera (Sony DCX-3000, Japan) connected to a microcomputer. A 1 mm core diameter fiber was mounted on the camera port of the microscope to collect fluorescence light from a 40 μm diameter micro-spot of the skin tissue section. The collected fluorescence light is then transmitted to an OMA for spectral analyses. The alignment of the fiber end to collect fluorescence light from a specific microlocation on the tissue slide was accomplished by connecting the fiber to an auxiliary alignment light source. A total of 30 sections from three normal human skin tissue samples were examined and all demonstrated similar results.

3. The optical model of human skin

Skin has a very complex structure and thus, for theoretical modeling, a simplified seven layer skin optical model was developed that related to the anatomical structure [18] and to the available intrinsic optical parameters of skin [8,9].

Table 1
The seven-layer skin optical model. The transport parameters (μ_a, μ_s, g) are for 442 nm only

Layer	d (μm)	n	μ_a (cm^{-1})	μ_s (cm^{-1})	g
Air	–	1.0	–	–	–
Stratum corneum	10	1.45	190	2300	0.9
Epidermis	80	1.4	56	570	0.75
Papillary dermis	100	1.4	6.7	700	0.75
Upper blood plexus	80	1.39	67	680	0.77
Reticular dermis	1500	1.4	6.7	700	0.75
Deep blood plexus	70	1.34	541	520	0.96
Dermis	160	1.4	6.7	700	0.75
Subcutaneous fat	–	1.46	–	–	–

Table 1 outlines this model by providing data for the thickness (d), refractive index (n), and the transport parameters (μ_a, μ_s, g) at 442 nm for each skin layer. For this study, 442 nm is the wavelength of the laser light used for fluorescence excitation in practice. The total thickness of the skin model is 2 mm, while the thickness of each layer is based on our microscopic measurements from skin tissue sections [17,19]. Externally, the skin is in contact with air (refractive index of 1.0), while internally, the skin is in contact with the subcutaneous fat which has a refractive index of 1.46 [20]. The refractive index of the stratum corneum was taken to be 1.45 [21]. For both the epidermis and the bloodless dermis, the refractive index was assumed to be 1.4 based on a water content of 70–80% [22]. The refractive index of blood was assumed to be 1.33, i.e. the same as that of water. The transport parameters for the stratum corneum, epidermis, and bloodless dermis were obtained from the literature [9]. The upper blood plexus consists of capillaries scattered inside the dermal tissue. Therefore, it was modeled to consist of a uniform layer of 10% blood and 90% dermal tissue in the optical model. The lower blood plexus was assumed to contain 90% blood and 10% dermal tissue because of the larger vessels at this site. The optical parameters (μ_a, μ_s, g, n) of the upper and lower blood plexus were calculated by adding the fractional contributions of their components [23]. For example, the refractive index of the upper blood plexus was estimated as

$$n = 1.4 \times 0.90 + 1.33 \times 0.10 = 1.39$$

These calculations can also be expressed by the following matrix formula:

$$\begin{bmatrix} \mu_a \\ \mu_s \\ g \\ n \end{bmatrix} = \begin{bmatrix} \mu_a^1 & \mu_a^2 \\ \mu_s^1 & \mu_s^2 \\ g^1 & g^2 \\ n^1 & n^2 \end{bmatrix} \times \begin{bmatrix} f_1 \\ f_2 \end{bmatrix} \quad (1)$$

where f_1 and f_2 are the percentages of two components, 1 and 2. Superscripts 1 and 2 in the first matrix on the right side denote the optical properties of component 1 and 2, respectively. The absorption coefficients of blood were obtained

from [24] and its μ_s value was assumed to be 500 cm^{-1} at 442 nm and in the wavelength range from 470 nm to 750 nm. This assumption is inconsistent with Mie theory since the sizes of blood cells (erythrocytes, 6.5 μm to ~8 μm, leukocytes, 6 μm to ~20 μm) [25] are much larger than the wavelengths of light of interest in this study (0.442 μm to 0.75 μm).

To model the fluorescence escape process, transport parameters (μ_a, μ_s, g) for the skin model at other wavelengths are also required. We compiled the data of each skin layer at 29 different wavelengths from 470 to 750 nm in 10 nm intervals using the data from the literature [9,24] and the method outlined for 442 nm. At some wavelengths, the parameters of the stratum corneum were not available, and in these instances, we assumed that its optical parameters were the same as those of the remainder of the epidermis. Table 2 shows example data for 520 nm.

Table 2
The transport parameters (μ_a, μ_s, g) at 520 nm of the seven-layer skin optical model

Layer	d (μm)	n	μ_a (cm^{-1})	μ_s (cm^{-1})	g
Air	–	1.0	–	–	–
Stratum corneum	10	1.45	40	570	0.77
Epidermis	80	1.4	40	570	0.77
Papillary dermis	100	1.4	5	500	0.77
Upper blood plexus	80	1.39	24.5	500	0.79
Reticular dermis	1500	1.4	5	500	0.77
Deep blood plexus	70	1.34	181	500	0.96
Dermis	160	1.4	5	500	0.77
Subcutaneous fat	–	1.46	–	–	–

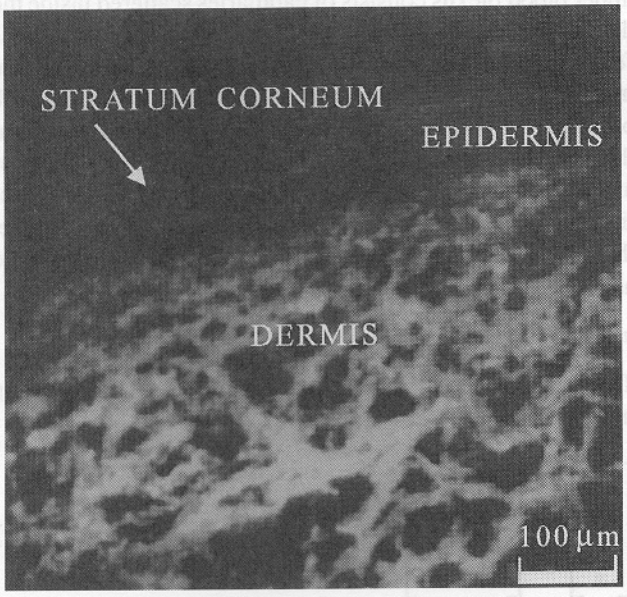

Fig. 1. Typical autofluorescence image of excised skin tissue sections obtained by a microspectrophotometer under 442 nm laser light excitation. The stratum corneum, the epidermis, and the dermis are well distinguished in the image. The dermis fluoresces brightly, the stratum corneum fluoresces with a weak signal, while the remaining epidermis yields even less autofluorescence.

Our previous studies have defined the fluorescence properties of the biopsied skin tissue sections [7,10,11,17,19]. Fig. 1 shows a typical autofluorescence image of a skin tissue section obtained by a microspectrophotometer (MSP) [17] with a CCD camera under 442 nm He–Cd laser light excitation. The original image is an RGB color image, while Fig. 1 is a gray scale image representing the average intensity distribution of the R, G, B signals. The figure shows that the skin fluorophore distribution is not uniform, but has a layered structure. The dermis fluoresces very strongly, the stratum corneum fluoresces with a weak signal, while the remainder of the epidermis yields even less autofluorescence. For simplicity, the fluorophore distribution can be considered uniform within a layer. Therefore, the fluorophore density function $\rho(x, y, z)$, in units of cm^{-3}, becomes dependent on z only and can be denoted as $\rho(z)$ in units of cm^{-1}. The z axis is perpendicular to the skin surface and represents the depth within the skin, the x, y axes are in the plane of the skin surface. Based on the average intensity of each layer shown in Fig. 1, we obtained the relative $\rho(z)$ in relative units shown in Fig. 2. The dermis fluoresces 7.5 times brighter than the

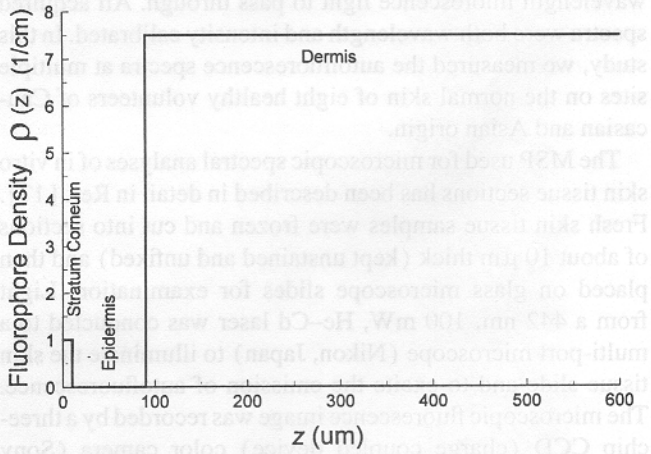

Fig. 2. Relative fluorophore density, ρ, as a function of depth, z, inside the skin tissue.

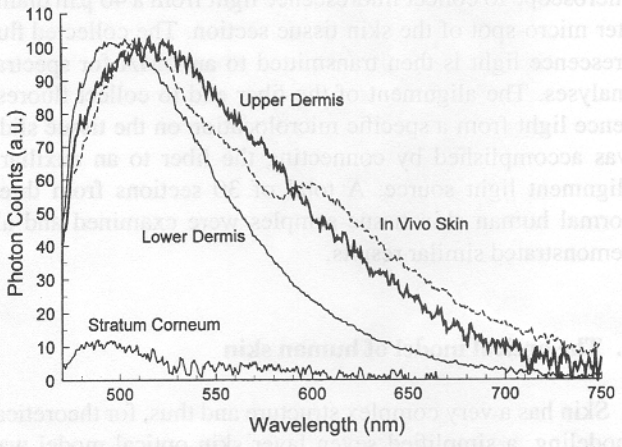

Fig. 3. The intrinsic autofluorescence spectra of skin fluorophores at different skin layers obtained by the MSP measurements. The average in vivo spectrum is also shown for comparison.

stratum corneum, while the remainder of the epidermis has negligible fluorescence.

Fig. 3 shows the intrinsic spectra of fluorophores at different skin layers obtained by the MSP measurements [7] along with the average in vivo skin autofluorescence spectrum curve for comparison. The spectral shapes were very reproducible for the 30 samples examined. The intrinsic spectra for the lower dermis ($z > 570$ μm) and upper dermis ($z < 570$ μm) are quite different. The average peak position of the upper dermis is 518 ± 2 nm, while the average peak position of the lower dermis is 497 ± 2 nm. However, as demonstrated below, very little 442 nm laser light reaches the lower dermis. Therefore, only the intrinsic spectra of stratum corneum and upper dermis are actually required for this work. However, the skin model still needs to include the lower dermis, since the fluorescence photons generated with longer wavelengths can penetrate into the lower dermis.

4. Methodology of reconstruction

The following procedure was used to reconstruct the in vivo skin autofluorescence spectrum using measured microscopic properties of skin tissue:

1. *Calculating the excitation light distribution inside the model skin.* The distribution of excitation light within the tissue must be specified. This was calculated using the Monte Carlo simulation, and is denoted as $\Phi(\lambda_{ex}, r, z, \theta)$ in units of W/cm^2. λ_{ex} is the excitation wavelength, while r, z, θ represent local positions in cylindrical coordinates.

2. *Obtaining the intrinsic fluorescence coefficient,* $\beta(\lambda_{ex}, \lambda_{em}, z)$. The intrinsic fluorescence coefficient β is defined as the product of the absorption coefficient due to the fluorophore, μ_{afl} (cm^{-1}), and the quantum yield Y (dimensionless) of fluorescence emission. Biological tissues like skin usually have a layered structure. Within a layer, β will be considered as a constant and can therefore be denoted as a function of z, $\beta(\lambda_{ex}, \lambda_{em}, z)$. λ_{em} is the wavelength of emitted fluorescence light. The product $\Phi\beta$ yields the density of fluorescence sources in units of W/cm^3. Using the MSP, one can measure the relative β distribution inside the tissue. The fluorophore density $\rho(z)$ can be calculated from the fluorescence image obtained by a CCD camera attached to the MSP. The intrinsic spectra of different tissue layers measured with MSP are normalized to equivalent overall integral intensity (the areas from 470 nm to 750 nm under each normalized intrinsic spectral curve are the same), and is denoted as $I_{norm}(\lambda_{ex}, \lambda_{em}, z)$, which is dimensionless. Then β can be obtained using

$$\beta(\lambda_{ex},\lambda_{em},z) = \rho(z) \times I_{norm}(\lambda_{ex},\lambda_{em},z) \quad (2)$$

3. *Calculation of Escape function* $E(\lambda_{em}, r, z)$. Once a fluorophore emits a fluorescence photon, that photon must reach the surface and escape to be observed. The escape function $E(\lambda_{em}, r, z)$ is the surface distribution as a function of radial position (r) of escaping photons from a point source of fluorescence at depth z and radial position $r = 0$ within a tissue of thickness D. It can be calculated by Monte Carlo simulation. The unit of E is cm^{-2}. Simulations were conducted for a series of depths (z) inside the tissue, using the optical properties for the emission wavelengths of interest.

4. *Calculation of the observed fluorescence,* $F(\lambda_{ex}, \lambda_{em}, r)$. The observed flux rate of escaping fluorescence F in units of W/cm^2 at the tissue surface is computed by the following convolution [4]:

$$F(\lambda_{ex},\lambda_{em},r) = \int_0^D \int_0^{2\pi} \int_0^{\infty} \Phi(\lambda_{ex},r',z',\theta)\,\beta(\lambda_{ex},r',z') \times E(\lambda_{em},\sqrt{r^2+r'^2-2rr'\cos\theta'},z')\,r'\,dr'\,d\theta'\,dz' \quad (3)$$

The convolution in Eq. (3) can be implemented numerically using discrete values for Φ and E that were generated by the Monte Carlo simulation, and the experimentally determined β.

We used the Monte Carlo code from Ref. [26] to calculate the excitation light distribution inside the model skin. To calculate the fluorescence escape function, the source code was modified to simulate the light propagation process for an isotropic fluorescence point source buried at depth z inside the tissue.

5. Results and discussion

Monte Carlo simulations were conducted to generate the fluence rate distributions inside the model skin for the 442 nm excitation laser light and for the escape functions for 40 different source depths and 29 different emission wavelengths from 470 nm to 750 nm. In each simulation, 1 000 000 photons were launched. In this work, the in vivo fluorescence spectra were measured using a wide beam illumination (1 cm diameter beam) and a small pick-up spot (3 mm diameter) at the center of the illumination field [6,10]. Therefore, the excitation light distribution could be simplified as a function of z only, i.e. $\Phi(z)$. For a wide illumination beam, the fluorescence intensity will be the same in the tissue surface independent of position r. In Eq. (3), the fluorescence escape function $E(\lambda_{em}, r, z)$ can be integrated with respect to r and θ first:

$$\iint E(\lambda_{em},r,z)\,r\,dr\,d\theta = E(\lambda_{em},z) \quad (4)$$

The contribution from a specific skin layer (from depth z_1 to depth z_2) to the observed in vivo fluorescence spectrum can be calculated as follows:

$$F_{\text{layer: } z_1 \to z_2}(\lambda_{ex},\lambda_{em}) = \int_{z_1}^{z_2} \Phi(z)\,\beta(\lambda_{ex},\lambda_{em},z)\,E(\lambda_{em},z)\,dz \quad (5)$$

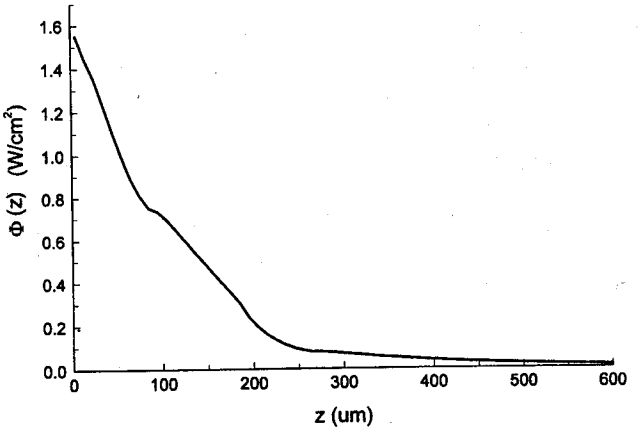

Fig. 4. The excitation light (442 nm) distribution as a function of depth z inside the skin tissue (infinite wide beam, normal incidence). The incident power density is 1 W/cm^2.

Note that, within a skin layer, β is assumed to be independent of depth. In this work, the excitation wavelength λ_{ex} is also fixed at 442 nm. Substituting λ_{em} with λ, Eq. (5) becomes

$$F_{\text{layer: } z_1 \to z_2}(\lambda) = \beta(\lambda) \int_{z_1}^{z_2} \Phi(z) E(\lambda, z)\, dz \tag{6}$$

We call the integral on the right side of Eq. (6) the fluorescence detection efficiency, $\eta_{\text{layer: } z_1 \to z_2}$, which represents the likelihood of obtaining an autofluorescence signal from a specific skin layer.

$$\eta_{\text{layer: } z_1 \to z_2}(\lambda) = \int_{z_1}^{z_2} \Phi(z) E(\lambda, z)\, dz \tag{7}$$

It is an integral of the product of the excitation light distribution inside the tissue and the fluorescence escape efficiency. The reconstructed skin in vivo spectrum is a linear combination of the product of intrinsic spectrum and the fluorescence detection efficiency of all the excited fluorophores:

$$F(\lambda) = \beta_{\text{stratum corneum}}(\lambda)\, \eta_{\text{stratum corneum}}(\lambda) + \beta_{\text{dermis}}(\lambda)\, \eta_{\text{dermis}}(\lambda) \tag{8}$$

Fig. 4 shows the excitation light distribution as a function of depth z for incident power density of 1 W/cm^2. It can be seen that very little light penetrates into the lower dermis ($z > 570$ μm). The stratum corneum and the papillary dermis contribute the most to the in vivo fluorescence signal.

Fig. 5 shows the calculated fluorescence escape efficiency $E(\lambda, z)$ as a function of wavelength for different depths z inside the tissue. Near the tissue surface, $E(\lambda, z)$ vs. λ curves are flat and horizontal indicating that the reabsorption and scattering of the tissue to fluorescence photons have minimum effect on the fluorescence escape function. As the fluorescence sources appear deeper inside the tissue, the reabsorption and scattering of the fluorescence photons by the tissue have larger and larger effect on the fluorescence

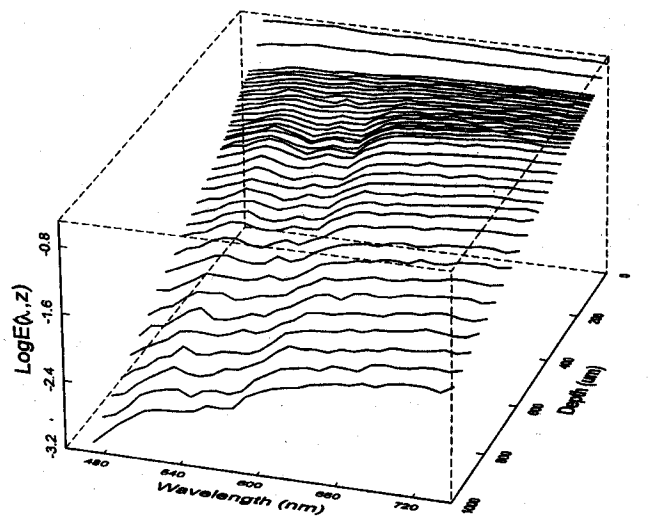

Fig. 5. Fluorescence escape efficiency, $E(\lambda, z)$, as a function of wavelength at different depth z inside the tissue calculated by Monte Carlo simulation for the model skin. A simulation was done for the stratum corneum layer (10 μm thick) at $z = 5$ μm. A single simulation was done for the 80 μm thick epidermis (at $z = 45$ μm) because there are few fluorophores in this layer. Thirty-eight simulations were done for the dermis. From $z = 90$ μm to $z = 270$ μm, simulations were done at 10 μm intervals; from $z = 270$ μm to $z = 510$ μm, at 15 μm intervals; and from $z = 510$ μm to $z = 1000$ μm, at 25 μm intervals.

escape function. $E(\lambda, z)$ vs. λ curves become more and more tilted as z increases, because both the absorption coefficient (μ_a) and the scattering coefficient (μ_s) of the skin tissue decrease with increasing wavelengths. The double absorption valleys of blood at 540 nm and 580 nm also become deeper at greater tissue depths. Fig. 6 shows the calculated fluorescence escape efficiency $E(\lambda, z)$ as a function of depth z inside the tissue at different wavelengths. The logarithm of $E(\lambda, z)$ decreases almost linearly with increasing depth within the tissue. The $E(\lambda, z)$ vs. z curve decays faster at short wavelengths indicating that fluorescence photons with short wavelengths have greater difficulty escaping from the tissue than photons with longer wavelengths. This is due to the variation in the absorption coefficient (μ_a) and scattering coefficient (μ_s) of skin tissue, which decrease with increasing wavelengths.

Fig. 7 shows the calculated fluorescence detection efficiency, η, as a function of wavelength for both the upper dermis and the stratum corneum. The effect of absorption by blood is clearly seen on the η_{dermis} curve, while the $\eta_{\text{stratum corneum}}$ curve is a relatively flat horizontal line showing that the absorption of melanin found in the epidermal layer and the absorption by blood in the dermis layer have little effect on the escape of the stratum corneum fluorescence due to the surface position of this thin tissue layer. The $\eta(\lambda)$ vs. λ curves represent how the intrinsic fluorescence spectra are distorted by the tissue reabsorption and scattering.

Fig. 8 shows the calculated skin autofluorescence spectrum in comparison with the experimental in vivo spectra. For different volunteers or different body locations on one volunteer, the in vivo skin autofluorescence intensity changed

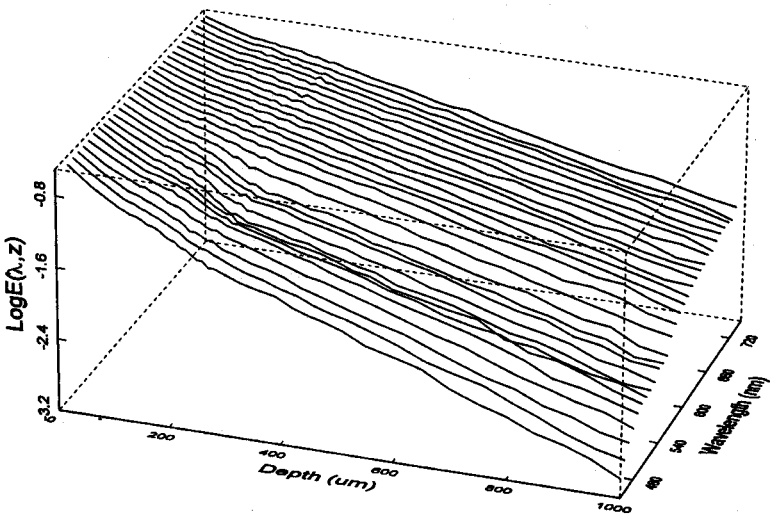

Fig. 6. Fluorescence escape efficiency, $E(\lambda, z)$, as a function of depth within the tissue at different wavelengths as calculated by Monte Carlo simulation for the skin model. The logarithm of $E(\lambda, z)$ decays almost linearly with increasing tissue depth z.

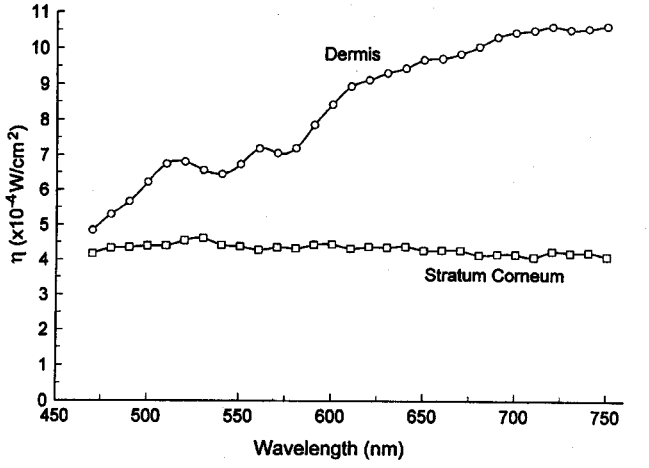

Fig. 7. Fluorescence detection efficiency η as a function of wavelength for the dermis layer and the stratum corneum layer.

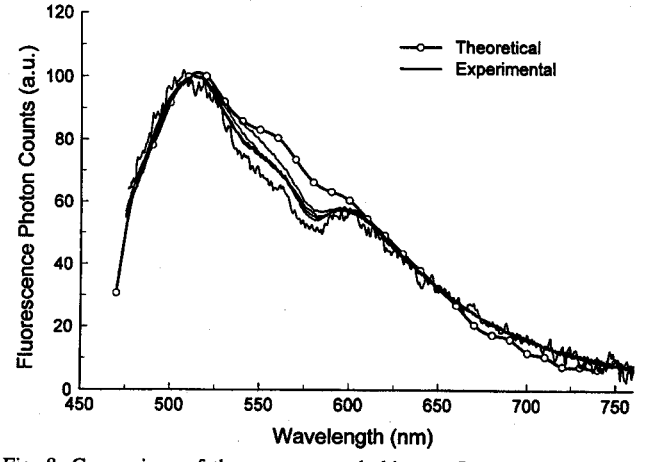

Fig. 8. Comparison of the reconstructed skin autofluorescence spectrum curve with the experimental in vivo data.

significantly (as much as 100%), but the spectral maximum position (wavelength) did not vary significantly (515 ± 2 nm), while the details of the spectral shape did change as a consequence of tissue reabsorption of the fluorescence light and the variation in the amount of the various absorption chromophores at different body locations or from subject to subject. Fig. 8 shows five experimental curves from two volunteers (one Asian, one Caucasian) and three different body locations (inner forearm: upper and lower positions, and hand dorsum). Each curve is normalized to have a maximum intensity of 100 counts. The blood absorption has much larger effect on the spectral shape than melanin does for fair colored Caucasian and Asian volunteers. The effect of the absorption on fluorescence light by blood can be seen in both the experimental curve and the reconstructed curve. Below 530 nm and above 600 nm, the theoretical curve fits quite close to the experimental curves. In these two wavelength bands (470–530 nm and 600–750 nm), light absorption by blood is relatively small compared to light absorption by tissue. However, big differences between the experimental curves and the theoretical curve exist over the strong haemoglobin absorption wavelength range (530–590 nm). This suggests that the theoretical method employed in this work, the published skin optical properties, and the microscopic fluorescence properties determined by our MSP measurements are basically correct. However, the assumptions in the skin model for the blood content amount, its distribution within the tissue model, and the oxyhaemoglobin/haemoglobin ratio may not truly represent the actual situation in the in vivo skin. An additional factor is that the amount of blood and its oxygenation state in tissue may also be highly dynamic. The effects of blood on tissue optical properties and tissue optical behavior deserve further investigation.

As noted in Fig. 3, the spectral shape of the in vivo skin is quite different from the intrinsic spectra of both the stratum corneum and the upper dermis. The in vivo spectrum is the intrinsic spectrum modified by tissue optical properties due to light–tissue interactions. These interactions include absorption and scattering which determine the excitation light distribution inside the tissue and affect the escape process of

the fluorescence photons. The modifications are represented by the fluorescence detection efficiency η as defined in Eq. (7). η can be calculated independent of the intrinsic spectra and represents the effects of tissue optics on fluorescence detection. The theoretical reconstruction in this work correctly accounted the light-tissue interactions (scattering, absorption, and regenerating of fluorescence photons). Therefore, outside of the strong blood absorption wavelength band, the theoretical curve is consistent with the experimental data.

Acknowledgements

This work was supported in part by the Medical Research Council of Canada and the National Cancer Institute of Canada. The authors wish to thank Drs. Steven L. Jacques and Lihong Wang of the University of Texas M.D. Anderson Cancer Center for providing the original Monte Carlo code.

References

[1] S. Chandrasekhar, Radiative Transfer, Dover Press, New York, 1960.
[2] A. Ishimaru, Wave Propagation and Scattering in Random Media, vol. 1, Academic Press, New York, 1978.
[3] R.R. Anderson, In vivo fluorescence of human skin, Arch. Dermatol. 125 (1989) 999.
[4] M. Keijzer, R. Richards-Kortum, S.L. Jacques, M.S. Feld, Fluorescence spectroscopy of turbid media: autofluorescence of the human aorta, Appl. Opt. 28 (1989) 4286–4292.
[5] R. Richards-Kortum, A. Metha, G. Hayes, R. Cothren, T. Kolubayev, C. Kittrell, N.B. Ratliff, J.R. Kramer, M.S. Feld, Spectral diagnosis of atherosclerosis using an optical fiber laser catheter, Amer. Heart J. 118 (1989) 381–391.
[6] H. Zeng, C. MacAulay, B. Palcic, D.I. McLean, A computerized autofluorescence and diffuse reflectance spectroanalyser system for in vivo skin studies, Phys. Med. Biol. 38 (1993) 231–240.
[7] H. Zeng, C. MacAulay, D.I. McLean, B. Palcic, Spectroscopic and microscopic characteristics of human skin autofluorescence emission, J. Photochem. Photobiol. 61 (1995) 639–645.
[8] R.R. Anderson, J.A. Parrish, Optical properties of human skin, in: J.D. Regan, J.A. Parrish (Eds.), The Science of Photomedicine, Plenum Press, New York, 1982, pp. 147–194.
[9] M.J.C. Van Gemert, S.L. Jacques, H.J.C.M. Sterenborg, W.M. Star, Skin optics, IEEE Trans. Biomed. Eng. 36 (1989) 1146–1154.
[10] H. Zeng, C. MacAulay, B. Palcic, D.I. McLean, Laser-induced changes in autofluorescence of in vivo skin, SPIE Proc. Laser–Tissue Interaction IV 1882 (1993) 278–290.
[11] H. Zeng, Human skin optical properties and autofluorescence decay dynamics, Ph.D. Thesis, The University of British Columbia, Vancouver, BC, Canada, 1993.
[12] R. Richards-Kortum, R.P. Rava, M. Fitzmaurice, L. Tong, N.B. Ratliff, J.R. Kramer, M.S. Feld, A one-layer model of laser induced fluorescence for diagnosis of diseases in human tissue: applications to atherosclerosis, IEEE Trans. Biomed. Eng. 36 (1989) 1222–1232.
[13] R.J. Crilly, W.F. Cheong, M. Motamedi, J.R. Spears, Simulation of fluorescent measurements in a turbid media, Laser Surg. Med., Suppl. 4 (1992) 4.
[14] C.M. Gardner, S.L. Jacques, A.J. Welch, Fluorescence and reflectance spectra specify intrinsic fluorescence spectrum corrected for tissue optics distortion, SPIE Proc. 1885 (1993) 122–128.
[15] E. Tinet, S. Avrillier, Monte Carlo modelisation of laser induced fluorescence signals in turbid media: determination of original fluorescence spectra, SPIE Proc. 1887 (1993) 69–76.
[16] J. Qu, C. MacAulay, S. Lam, B. Palcic, Laser-induced fluorescence spectroscopy at endoscopy: tissue optics, Monte Carlo modeling, and in vivo measurements, Opt. Eng. 34 (1995) 3334–3343.
[17] H. Zeng, C. MacAulay, D.I. McLean, B. Palcic, Novel microspectrophotometer and its biomedical applications, Opt. Eng. 32 (1993) 1809–1814.
[18] W. Montagna, A.M. Kligman, K.S. Carlisle, Atlas of Normal Human Skin, Springer-Verlag, New York, 1992.
[19] H. Zeng, C. MacAulay, B. Palcic, D.I. McLean, Autofluorescence distribution in skin tissue revealed by microspectrophotometer measurements, SPIE Proc. 1876 (1993) 129–135.
[20] F.P. Bolin, L.E. Preuss, R.C. Taylor, R.J. Ference, Refractive index of some mammalian tissue using a fiber optic cladding method, Appl. Opt. 28 (1989) 2297–2303.
[21] J.L. Solan, K. Laden, Factors affecting the penetration of light through stratum corneum, J. Soc. Cosmet. Chem. 28 (1977) 125–137.
[22] B.C. Wilson, S.L. Jacques, Optical reflectance and transmittance of tissue: principles and applications, IEEE J. Quantum Electron. 26 (1990) 2186–2198.
[23] S.L. Jacques, S. Rastegar, M. Motamedi, S.L. Thomsen, J. Schwartz, J. Torres, I. Mannonen, Liver photocoagulation with diode laser (805 nm) vs. Nd:YAG laser (1064 nm), SPIE Proc. 1646 (1992) 107–117.
[24] S.L. Jacques, M. Keijzer, Dosimetry for lasers and light in dermatology – Monte Carlo simulation of 577 nm pulsed laser penetration into cutaneous vessels, SPIE Series 1422 (1991) 2–13.
[25] L.C. Junqueira, J. Carneiro, R.O. Kelley, Basic Histology, Appleton & Lange, Norwalk, CT, 1989, p. 235.
[26] L. Wang, S.L. Jacques, Monte Carlo modeling of light transport in multilayered tissue in standard C, University of Texas M.D. Anderson Cancer Center, Houston, TX, 1992.